UCRL-17877

c. 2

University of California

Ernest O. Lawrence Radiation Laboratory

ANGULAR CORRELATION- AND MÖSSBAUER-NMR

E. Matthias

October 1967

DISCLAIMER

(Paper for the International Conference on Hyperfine Interactions Detected by Nuclear Radiation, August 25-30, 1967, Asilomar)

UCRL-17877
Preprint

UNIVERSITY OF CALIFORNIA

Lawrence Radiation Laboratory
Berkeley, California

AEC Contract No. W-7405-eng-48

ANGULAR CORRELATION- AND MÖSSBAUER-NMR

E. Matthias

October 1967

ANGULAR CORRELATION- AND MÖSSBAUER-NMR

E. Matthias

Lawrence Radiation Laboratory
University of California
Berkeley, California

ABSTRACT: The general question of how to perform and detect nuclear magnetic resonance in radioactive isotopes is discussed. The paper will focus on γ-ray detection of resonances in isomeric states. The use of multipole radiation fields for detection introduces new and hitherto unobserved line shapes. For rf with random phase, the resonance line is k-fold split, where k is the summation index of the Legendre polynomial expansion. If pulsed rf with a constant phase is used, form and symmetry of the resonances depend strongly upon the phase and the geometry of the experiment. The existence of a "hard core" value at resonance frequency is demonstrated. Various geometries are examined with respect to their applicability in angular correlation or nuclear reaction experiments. The possibility of obtaining the relative sign of gH with respect to a reference case at certain geometries and by using linearly polarized rf with a fixed phase is discussed.

Gamma ray detection of NMR is not only restricted to angular correlations and distributions but can also be performed by employing the Mössbauer effect. The principle is discussed and preliminary results obtained with Fe^{57} are presented. Although the NMR interpretation is likely, the data do not, at present, unambigously rule out the possibility of a frequency modulation effect.

I. INTRODUCTION

The subject Angular Correlation- and Mössbauer-NMR belongs in the more general category of nuclear magnetic resonance (NMR) in radioactive nuclear states, which has recently attracted the intensified interest of experimenters. Two reasons for this are obvious:

1. There is a vast number of isomeric nuclear states with half-lives between 10^{-6} s and 10^{2} s which are hardly accessible to conventional techniques and which offer a whole new field for the investigation of hyperfine interactions.

2. Standard methods like angular correlation and nuclear orientation have always suffered from being limited in their accuracy due to statistics. If NMR methods can be applied, the accuracy will be given mainly by the linewidth and statistics is only required for recognizing the line shape.

Classical detection methods cannot be used for short-lived radioactive states due to the extremely low concentration. The only possibility for detecting the resonance is to use the radiation pattern emitted from the state which is to be measured. It is important to notice that this constitutes a microscopic method in which a statistical assembly of nuclei is observed, as compared to the detection of macroscopic magnetization in conventional NMR work. The concept of radiative detection has been established by a number of original experiments which are listed in Table I in chronological order. Except for the cases 1, 3, 7, and 8, the β-asymmetry was used to observe the resonance, and the listed experiments of type 2., 5., and 6. therefore apply only to radioactive ground states and the few β-emitting isomeric states. There is, however, a great number of isomeric states which only decay by γ-ray emission. With this

in mind we shall discuss the possibilities of using γ-radiation as a means to detect the resonance. The following four techniques appear to be applicable for this task:

1. Angular correlations involving intermediate states with $10^{-8} < T_{1/2} < 10^{-5}$ s.

2. Angular distributions of γ-rays from isomeric states in the half-life range $10^{-8} < T_{1/2} < 10$ s, populated in nuclear reactions.

3. Nuclear orientation involving parent states with half-lives sufficiently long to permit orientation work ($T_{1/2} > 10$ hrs); and reorientation in intermediate states with $T_{1/2} \gtrsim T_1$ (T_1 = nuclear spin-lattice relaxation time).

4. Mössbauer effect in the half-life range 10^{-8} s $< T_{1/2}$.

In methods 1, 2, and 3 polarized or aligned nuclear states are obtained which emit non-isotropic γ-ray angular distributions of the general form

$$W(\Theta) = \sum_{k_{even}} C_k A_k P_k(\cos \Theta) \qquad (1)$$

The Mössbauer effect can be used because of its polarization dependence. Methods 1, 3, and 4 have been proven experimentally to be feasible, while there is not yet an experimental verification of method 2. In the present paper we will only discuss methods 1, 2, and 4. Nuclear orientation-NMR will be treated by D. A. Shirley in a separate paper.[9]

II. ANGULAR CORRELATION-NMR

Recently, it was proven[7] that the NMR can be measured in a state with a half-life as short as $2.3 \cdot 10^{-7}$ s by employing the hyperfine enhancement of the rf-field and detecting the resulting perturbation of an angular correlation involving this state. Some more mainly methodical studies have been carried out with the same case, ^{100}Rh, and are reported in these Proceedings.[10] However, ^{100}Rh has thus far remained the only successful case and it is an unfortunate fact that there are only very few prospective candidates for angular correlation-NMR with radioactive sources. Therefore, it is evident that the importance of this method will be its application to angular distributions following nuclear reactions. We will discuss below a few points which are characteristic for NMR observation with γ-multipole fields. For experimental details and general principles, the reader is referred to Ref. 10.

A. General Formalism

To describe the resonance behavior we start out with the general form of a perturbed angular correlation[11]

$$W(\vec{k}_1,\vec{k}_2,t) = \sum_{\substack{k_1 k_2 \\ N_1 N_2}} [(2k_1+1)(2k_2+1)]^{-1/2} A_{k_1}(1) A_{k_2}(2)\, G_{k_1 k_2}^{N_1 N_2}(t) \times Y_{k_1}^{N_1 *}(\theta_1,\phi_1)\, Y_{k_2}^{N_2}(\theta_2,\phi_2) \quad , \tag{2}$$

where the perturbation factor is given by

$$G_{k_1 k_2}^{N_1 N_2}(t) = [(2k_1+1)(2k_2+1)]^{1/2} \sum_{m_a m_b} (-1)^{2I+m_a+m_b} \begin{pmatrix} I & I & k_1 \\ m_a' & -m_a & N_1 \end{pmatrix} \times \begin{pmatrix} I & I & k_2 \\ m_b' & -m_b & N_2 \end{pmatrix} \langle m_b|\Lambda(t)|m_a\rangle \langle m_b'|\Lambda(t)|m_a'\rangle^* \quad (3)$$

The general geometry defining θ and ϕ is sketched in Fig. 1 for the case of linearly polarized rf along the x-axis.

The time evolution operator $\Lambda(t)$ can be derived by solving the Schrödinger equation

$$\frac{\partial \Lambda(t)}{\partial t} = -\frac{i}{\hbar} \mathcal{H}(t)\Lambda(t) \quad . \quad (4)$$

The Hamiltonian is time-dependent, and for circularly polarized rf of the form

$$\mathcal{H}(t) = -g\mu_N[H_0 I_z + H_1(I_x \cos(\omega t+\Delta) \pm I_y \sin(\omega t+\Delta))] \quad (5)$$

The phase Δ accounts for the fact that the nuclear state which is formed at t=0 has an arbitrary phase angle Δ with respect to the rf. If continuous rf is used one has to average over the phase Δ.

We shall follow here the usual practice to solve Eq. (4) by transforming into a rotating coordinate system, S', in which the Hamiltonian is no longer time-dependent. The unitary transformation

$$\Lambda(t) = U(t)\,\Lambda'(t)\,U^{\dagger}(0) = e^{\mp iI_z(\omega t+\Delta)}\, e^{-\frac{i}{\hbar}\mathcal{H}'t}\, e^{\pm iI_z\Delta} \quad (6)$$

leads to a static Hamiltonian in the rotating frame of the form

$$\mathcal{H}' = -g\mu_N[(1 \pm \frac{\omega}{\omega_L})H_0 I_z + H_1 I_x] \tag{7}$$

with the usual definition: $\omega_L = g\frac{\mu_N}{\hbar} H_0$. Inserting Eq. (6) into Eq. (3) gives for the general perturbation factor

$$G^{N_1 N_2}_{k_1 k_2}(t) = [(2k_1+1)(2k_2+1)]^{1/2} \sum_{m_a m_b} (-1)^{2I+m_a+m_b} \begin{pmatrix} I & I & k_1 \\ m'_a & -m_a & N_1 \end{pmatrix} \begin{pmatrix} I & I & k_2 \\ m'_b & -m_b & N_2 \end{pmatrix}$$

$$\times e^{\mp i\omega t N_2} \; e^{\mp i(N_2-N_1)\Delta} \langle m_b | e^{-\frac{i}{\hbar}\mathcal{H}'t} | m_a \rangle \langle m'_b | e^{-\frac{i}{\hbar}\mathcal{H}'t} | m'_a \rangle^* \tag{8}$$

The Hamiltonian $\mathcal{H}'$ (Eq. (7)) is not diagonal in the above representation. It has to be diagonalized by another unitary transformation

$$S\mathcal{H}'S^{-1} = E \quad , \tag{9}$$

which results in

$$\langle m_b | e^{-\frac{i}{\hbar}\mathcal{H}'t} | m_a \rangle = \sum_n \langle n|m_b\rangle^* e^{-\frac{i}{\hbar}E_n t} \langle n|m_a\rangle \quad . \tag{10}$$

Consequently we obtain for the final form of the perturbation factor

$$G_{k_1k_2}^{N_1N_2}(t) = [(2k_1+1)(2k_2+1)]^{1/2} \sum_{\substack{m_a m_b \\ n\, n'}} (-1)^{2I+m_a+m_b} \begin{pmatrix} I & I & k_1 \\ m_a' & -m_a & N_1 \end{pmatrix} \begin{pmatrix} I & I & k_2 \\ m_b' & -m_b & N_2 \end{pmatrix} \tag{11}$$

$$\times \langle n|m_b\rangle^* \langle n|m_a\rangle \langle n'|m_b'\rangle \langle n'|m_a'\rangle^* e^{\mp i(N_2-N_1)\Delta} e^{-i\left[\frac{E_n-E_{n'}}{\hbar} \pm N_2\omega\right]t}$$

If the resonance is observed in a time-integral manner, the perturbation factor has to be integrated over the decay of the delayed state

$$\hat{G}_{k_1k_2}^{N_1N_2} = \frac{1}{\tau}\int_0^\infty G_{k_1k_2}^{N_1N_2}(t)\, e^{-t/\tau}\, dt \quad , \tag{12}$$

or explicitly:

$$\hat{G}_{k_1k_2}^{N_1N_2} = [(2k_1+1)(2k_2+1)]^{1/2} \sum_{\substack{m_a m_b \\ n\, n'}} (-1)^{2I+m_a+m_b} \begin{pmatrix} I & I & k_1 \\ m_a' & -m_a & N_1 \end{pmatrix} \begin{pmatrix} I & I & k_2 \\ m_b' & -m_b & N_2 \end{pmatrix}$$

$$\times \langle n|m_b\rangle^* \langle n|m_a\rangle \langle n'|m_b'\rangle \langle n'|m_a'\rangle^* e^{\mp(N_2-N_1)\Delta} \tag{13}$$

$$\times \frac{1 - i\{\frac{\tau}{\hbar}(E_n-E_{n'}) \pm N_2\omega\tau\}}{1 + \{\frac{\tau}{\hbar}(E_n-E_{n'}) \pm N_2\omega\tau\}^2}$$

C. Hard Core Value

The splitting of the resonance is a purely geometrical effect which goes together with another interesting fact, namely, the occurence of a "hard core" value at resonance. From Figs. 2, 3 and Fig. 9 of Ref. 10 it can be seen that a fraction of the anisotropy remains at resonance ($\omega=|\omega_0|$) no matter how large the imposed rf amplitude is. This hard core value at $\omega=|\omega_0|$ is again independent of the nuclear spin and given by the expression

$$\hat{G}_{kk}^{00}(\infty) = (k!)^2/(k!!)^4 \quad . \tag{14}$$

The power dependence shown in Fig. 8 of Ref. 10 shows how the perturbation factor behaves at resonance and for what power levels the hard core value is approached.

It is important to notice, however, that slightly off resonance the anisotropy can actually be wiped out completely (see Figs. 2 and 3) for sufficiently large amplitudes of H_1. This is expected since transitions induced by a strong rf-field resembles a situation very similar to the one of a random time-dependent perturbation, for which no hard core exists.[14]

The power requirement for obtaining a sizeable resonance effect is inversely proportional to the magnitude of $\omega_0\tau$. A plot of the perturbation factor $\hat{G}_{22}^{00}$ versus $\omega_0\tau$ has therefore a similar appearance as the power dependence. To mediate an impression about what can be done for a given half-life, the $\omega_0\tau$-dependence of $\hat{G}_{kk}^{00}$ is shown in Fig. 4 for three values of the power parameters H_1/H_0.

D. Experimental Geometries

To illustrate what is to be expected in an actual experiment we will discuss in the following the resonance behavior for specific geometrical arrangements of the detectors, the dc and ac fields. As mentioned above, one has to distinguish between two cases: 1) continuous rf, random in phase with respect to the nuclear decay, and 2) pulsed rf, triggered by the first gamma ray or the beam signal (to which it more realistically applies) with a constant phase angle Δ .

a. Continuous rf

In Table II some angular correlation formulas restricted to $k_{max} = 2$ are given for an arbitrary selection of geometries, described by (θ_1,ϕ_1) and (θ_2,ϕ_2)(cf. Fig. 1). Since the rf has no phase relation with respect to t = 0 one has to integrate over this phase angle Δ (cf. Eq. (13)). This integration leads to the fact, that the only non-vanishing terms are those with $N_1 = N_2$. All these terms are symmetric around $|\omega| = \omega_0$. In cases 1 through 5 it makes no difference to interchange γ_1 and γ_2.

For convenience we will consider only time-integrated values of the perturbation factor. Since $\mathrm{Re}\hat{G}_{22}^{NN}$ and also $\mathrm{Im}\hat{G}_{22}^{NN}$ are very small compared to $\hat{G}_{22}^{00}$ the numerical results for cases 3 through 7 are identical to better than 1% and given by $\frac{1}{4}\hat{G}_{22}^{00}$. Thus, by applying the proper scale factor the expected resonance behavior for all geometries listed in Table II can be obtained from Fig. 2. In all cases the resonance is split and shows the characteristic hard core.

It should be noticed, that the cases 5, 6, and 7 represent "easy" geometries for in-beam experiments with H_0 perpendicular to the beam. As

long as A_{22} is of reasonable size, it is perfectly feasible to perform resonance experiments in this way with isomeric states that are populated by nuclear reactions.

b. Pulsed rf and Sign Determination

For this section it is assumed that the rf is triggered phase-right by the process which populates the isomeric level and thus determines $t = 0$ or vice versa. It can be seen from Eq. (13) that the resulting angular correlation function is very crucially dependent upon the phase angle Δ at which the rf is turned on and also upon the geometry of the detectors. This gives rise to a complexity of possible line shapes which offer interesting features like relative sign determination and unsplit resonances. Further, we shall only discuss here cases for which $\Delta = 0$, assuming that this condition can always be met experimentally, for example, by synchronous pulsing of beam and rf.

The angular correlation functions with $k_{max} = 2$ are listed in Table III for some arbitrary geometries which might be of interest. Except for case 1, which is anyway independent of phase, the most marked feature of these formulas is that they contain terms with $N_1 \neq N_2$. These terms are in general not symmetric about the resonance and make the shape very much dependent on which terms are involved. For convenience we will abbreviate the correlation function in the common form

$$W(\vec{k}_1,\vec{k}_2,\vec{H}_0,\vec{H}_1) = 1 + A_{22}G_{22}^{eff}(\vec{k}_1,\vec{k}_2,\vec{H}_0,\vec{H}_1) \qquad (15)$$

and discuss the G_{22}^{eff} in the following figures. The cases selected for illustration are representative for the large number of possibilities listed in Table III.

Figure 5 shows the resonance which is to be expected in a 90°-geometry with γ_2 parallel to the dc magnetic field. The marked feature is the asymmetry about $\omega = |\omega_0|$ for opposite signs of $\omega_0\tau$ or, equivalently, two angles, 45°(225°) and 135°(315°). This can be used to determine the relative sign of $\omega_0\tau$ with respect to a reference case, even when linearly polarized rf is used. To do so, one has to observe the shift of the resonance at the two angles 45°(225°) and 135°(315°) and compare it with a case of known sign. In practice, this might be difficult since the shift is small and can only be picked up in experiments with great sensitivity and free of additional broadening. An absolute sign determination however, is still only possible with circularly polarized rf.

Another and more elegant way to obtain the relative sign of $\omega_0\tau$ is demonstrated in Fig. 6. This case is typical for how complex the resonance shape can become for "odd" geometries. With γ_2 again parallel to the dc-field and γ_1 detected at only <u>one</u> angle as indicated, the expected resonance effect, for example, for $-\omega_0\tau$ (and $-\omega/\omega_0$) first grows positive with increasing $\omega_0\tau$ and then decreases, turns negative and splits up. A comparison between $+\omega_0\tau$ and $-\omega_0\tau$ shows that the resonance effect has not only opposite sign for $|\omega_0\tau| < 10^4$ but also a remarkably different shape. For $|\omega\tau| \gtrsim 10^4$ the resonances for $+\omega_0\tau$ and $-\omega_0\tau$ become similar in form and approach each other numerically. Again, the opposite sign of the resonance can be employed to find the sign of $\omega_0\tau$ by comparison with a reference case.

The last three examples have been chosen as all having H_0 perpendicular to the detector plane. That is a convenient arrangement both for angular correlations and beam work. In Fig. 7 the simplest angular correlation case is shown. It offers the advantage that the center peak is considerably narrower compared with a normal resonance width which would allow a more accurate frequency determination. Beam-experiments with this particular geometry, however, are impossible because of intensity reasons. Figure 8 illustrates the fact that a clean unsplit resonance can be obtained at certain geometries and with a fixed rf phase. It so happens that the geometry in Fig. 8 also represents the most convenient detector arrangement in beam-experiments. The resonance shape for another geometry that can easily be applied to beam work is shown in Fig. 9. Here again one has the possibility to make a determination of the relative sign, provided the necessary sensitivity can be achieved.

The conclusion is that experiments with fixed-phase rf in relation to $t = 0$ are very appealing. Compared to measurements with random rf they offer attractive aspects such as relative sign determination and favorable line shapes. On the other hand, it may perhaps present experimental difficulties if not ambiguities that a great variety of resonance shapes can be obtained by only small changes in the phase or in angular positions.

III. MÖSSBAUER-NMR

A. General Consideration

The Mössbauer effect with polarized source and absorber is both direction- and polarization dependent and qualifies, for this reason, as a candidate for γ-ray detection of NMR. This possibility was first tested in 1960 by G. J. Perlow[3] who reported an increase of the transmission by 10% at 26 MHz, the ferromagnetic nuclear resonance frequency of the 14.4 keV level. To explain this effect, Hack and Hamermesh[13] calculated the effect of an rf-field on the form of the Zeeman lines, assuming that nuclear resonance transitions are induced. They showed that for a sufficiently large rf power level the lines split up as discussed above.

Despite this encouraging background apparently no further effort was devoted to the development of this experimental technique. This in spite of the fact, that the Mössbauer effect can, in principle, be observed by any technique which changes or modulates the energy of a Mössbauer system with sufficiently high sensitivity. The linear Doppler shift is only one possible way, another is to induce nuclear Zeeman transitions by an rf-field. In fact, the accuracy of the radiofrequency is much superior to what can be achieved with a velocity drive. This is best illustrated by an example: twice the natural linewidth of the 93 keV state in ^{67}Zn is 23.5 kHz or correspondingly 3.1×10^{-4} mm/sec. While it is very easy to obtain with common oscillators a stability which is at least an order of magnitude better than this expected linewidth, it is an extremely difficult task to achieve such resolution with a velocity spectrometer. For half-lives shorter than 10^{-7} sec, however, the NMR-method would not offer any advantage because of the large natural line-width.

Although determined to apply the Mössbauer-NMR technique to long-lived states, as for example, ^{181}Ta (6.3 keV) and ^{67}Zn (93.3 keV), we started out with ^{57}Fe to study the details of the method. The first preliminary results will be reported in the following.

B. Experimental Results

In all experiments described here a split source and absorber (^{57}Fe in Fe) was used, and the measurements were carried out at zero velocity. The source consisted of a solid solution of Co^{57} in Fe; the sample was rolled to a thickness of 1.2×10^{-4} cm. The absorber was a 2.4×10^{-4} cm thick Fe-foil enriched to 90% in ^{57}Fe. A split source and absorber was chosen since for these experiments the rf field should be sufficiently large to make the transition probability between the nuclear Zeeman levels (proportional to H_1^2) approximately equal to the decay probability of the excited state. To achieve this, again use was made of the hyperfine enhancement factor,[15] which is for domains

$$H_1^{eff} = \left(1 + \frac{H_{hf}}{H_o}\right) H_1^{osc}, \tag{16}$$

where H_{hf} is the magnetic hyperfine field.

Unless otherwise stated, source and absorber were rigidly affixed together and placed within a shielded rf helix which was held between the pole tips of a 4 in. diameter electromagnet. The dc magnetic field, H_o, and the rf field, H_1, were both in the plains of the foils, perpendicular to each other and perpendicular to the γ-ray propagation direction. A Si(Li) detector

counted the 14.4 keV gammas in transmission. In this geometry the full Mössbauer effect was obtained as source and absorber hyperfine lines overlap. The procedure was to measure the counting rate as a function of applied frequency. The frequencies of the expected resonances are well known: the ground state NMR has been measured directly and occurs at 45.44 MHz at room temperature;[15] the excited state resonance is expected at 25.98 MHz based on the ratio of magnetic moments as determined from Mössbauer effect data.[16]

The experimental results are shown in Figs. 10, 11 and 12. A coarse scan of the frequency range between 18 MHz and 49 MHz is displayed in Fig. 10. At the expected nuclear resonance frequencies a marked deviation from the general background behavior is observed. In Figs. 11 and 12 the resonances of the 14.4 keV state and of the ground state respectively, have been remeasured with better statistical accuracy. The line width obtained agrees well with the one expected from the natural width, $\Delta\nu = (\pi\tau)^{-1} = 2.3$ MHz. Also, it can be noticed that the ground state resonance is much less pronounced compared to the excited state resonance. This is probably caused by two effects, its four times smaller statistical weight factor and the different background situation at this higher frequency.

From the various measurements the following empirical conclusions can be derived:

1. There is a very strong non-resonant background effect in that sense that the Mössbauer effect is partially destroyed by application of an rf field. The background varies approximately exponentially with frequency in the range of interest. Since the absorber has a thickness of 2.4×10^{-4} cm and the skin depth for iron at 26 MHz is 2.2×10^{-4} cm, this exponential background behavior

must be interpreted as being related to the skin-depth. Further, the background effect depends strongly on H_o and H_1. Increasing H_o partially restores the Mössbauer effect, as can be seen from Fig. 13. Increasing the rf amplitude, H_1, shows the opposite result.

2. At the nuclear resonance frequency a fraction of the Mössbauer effect is restored, indicating that induced nuclear magnetic resonance transitions compensate for the background effect. This resonance behavior around 26.0 MHz and 45.4 MHz has at present been reproduced with two different sources and several absorbers under the same general conditions. However, form and the surface condition of both sources were different. The magnitude of this resonance effect decreases with increasing H_o (see Fig. 13) and increases with increasing H_1.

3. Only the ground state and the excited state resonance is observed. Although searched for, we were hitherto unable to find resonances at possible "beat" frequencies of 19.5 MHz and 52.0 MHz.

4. The nuclear magnetic resonance effect occurs already at surprisingly low H_1 amplitudes corresponding to, e.g., $\omega_1\tau = 0.35$ in Fig. 10.

5. The resonance has also been observed with either the absorber or the source alone exposed to the rf-field. However, the effect is somewhat smaller compared with the one obtained with both source and absorber in the rf-coil.

6. When the rf was applied to either source or absorber, the magnitude of the resonance effect was considerably larger in the case of perpendicular polarization than it was for parallel polarization of source and absorber. This is illustrated in Fig. 14.

C. Interpretation

The basic problem is whether the experimentally observed resonance effects are actually caused by induced nuclear magnetic resonance transitions. Another possible mechanism is frequency modulation caused by magnetostrictive motion in the source.[17] These two possibilities will be briefly discussed in the following.

a. Magnetostrictive Frequency Modulation.

Ruby and Bolef[18] showed that it is possible to create acoustically modulated gamma rays. They placed the source foil onto a piezoelectric quartz crystal which was driven by a 20 MHz radiofrequency, and observed with increasing driving amplitude the growing-in of sidebands, characteristic for frequency modulation. Unsplit source and absorber were used for their experiment. The sidebands occur at frequency intervals given by the modulation frequency only. Their intensity is determined by the corresponding Bessel functions of the first kind, and the argument of the Bessel functions is the modulation index which is proportional to the amplitude of the modulating rf. Therefore, an increasing rf amplitude will generate new sidebands. A similar situation can be imagined in our case. Magnetostriction produces microscopic motion which could be adequate to impart a modulation to the γ-rays. If source and absorber are not or only partly polarized, a sideband at 26 MHz would be matched by a Zeeman component of the γ-ray. The same argument would apply to the ground state frequency of 45.4 MHz. In the same way, however, other resonance effects should be found at 19.5 MHz, 52 MHz, etc. It is important to notice, however, that the frequency modulation picture produces the nuclear resonance frequencies only in case of random polarization. No resonances would occur at 26 MHz and

45.4 MHz for a completely polarized source and absorber. Since magnetostriction does generate a whole spectrum of velocities throughout the sample, the intensity of the sidebands will be appreciably reduced compared with the ideal case.

The following experimental observations provide evidence against magnetostriction: 1. A velocity spectrum was taken with a single line source and a split absorber. With the unpolarized absorber (H_0=0) exposed to an rf field of about 4G, no additional peaks due to sidebands could be found for example at 14.9 MHz. 2. Satellite resonances at 19.5 MHz and 45 MHz were carefully looked for but could not be verified. 3. From Fig. 13 it can be seen that even at H_0 = 1000 G, which should be sufficient to magnetically saturate the foils, a sizeable resonance was obtained. 4. The background for frequency modulation should be different from what was observed. When source and absorber are sandwiched inside the rf-coil, it is reasonable to assume that both are equally strong modulated by magnetostrictive motion. In the ideal case of equal thickness for source and absorber the absorption background should be independent of frequency at zero velocity. A difference in thickness causes the background to change with frequency as long as the thicknesses for source and absorber are of the same order of magnitude as the skin-depth. In the experiments presented in Figs. 10 to 13, source and absorber were 1.2×10^{-4} cm and 2.4×10^{-4} cm, respectively, compared to a skin depth of 2.2×10^{-4} cm at 26 MHz. For this we expect a constant or even slightly decreasing absorption background in sharp contrast to what is measured.

These arguments force us to reject magnetostrictive frequency modulation as an interpretation of the observed resonances. However, it is still

possible that this mechanism contributes to a certain extent and an unambiguous experiment to decide this question is still to be carried out.

b. Nuclear Magnetic Resonance.

The alternative explanation of the experimental results is that they actually represent rf-induced nuclear resonance transitions. In order to account for both the non-resonant background behavior and the resonance effect we have to assume a superposition of two effects: a periodic motion of the magnetization in the rf-field and, caused by this, induced Zeeman transitions at the nuclear resonance frequencies.

In the frequency range of interest here, the magnetization follows adiabatically with the rf-field. For small polarizing fields only the magnetization of the walls will vary periodically since the domains are shielded while for a magnetically saturated foil only domains need to be considered. The oscillating magnetization gives rise to an oscillating hyperfine field $H_1^{eff} = (1 + \frac{H_{hf}}{H_0}) H_1^{osc}$.[19] Since the Mössbauer absorption is very sensitive with regard to the polarization properties of the γ-rays, the relative orientation of $\vec{H}_{hf} = \vec{H}_{hf,z} + \vec{H}_1^{eff}(t)$ in source and absorber is very crucial. The skin-depth introduces a phase shift which means that the orientation of the hyperfine field varies with penetration depth. At lower frequencies in particular, where the half life is comparable with the inverse frequency, this has the consequence that the polarization direction of source and absorber only partly match (same depth layer) for a γ-ray emitted at time t. The result is that a good fraction of the Mössbauer absorption is lost. With increasing frequency, however, it will be restored since the penetrability for the rf becomes smaller and the originally matched polarization is not disturbed.

This concept explains the background behavior and links it both to the skin depth and to the comparable magnitude of half life and inverse frequency. It also accounts for the fact that the background slopes much less when only the source is inside the rf-field (Fig. 14) compared to the case where both source and absorber are in the rf-field (Fig. 10). For very long half lives there should be no rf-effect on the background under otherwise similar circumstances which provides a possibility of testing these ideas. Another conclusion of this interpretation is that there is always some fraction of the Mössbauer absorption left, which depends on source and absorber thickness and the skin depth. A measurement of the velocity spectrum with polarized split source and absorber would reveal whether or not our explanation of the non-resonant background behavior is correct.

At the nuclear resonance frequency the periodic motion of the magnetization is coherent with the Larmor precession of the nuclear spin system in the dc-polarized hyperfine field, H_{hf},z. The nuclei are exposed to an effective rf-field H_1^{eff}, which induces nuclear Zeeman transitions ($\Delta M = \pm 1$). At this point we have to assume that with the low power levels in question here, transitions are induced in either source or absorber (when sandwiched) but not in both.

Let us first consider the effect for source and absorber perpendicularly polarized and only the source exposed to the rf-field. This situation applies to the upper data set of Fig. 14. For simplicity we will also assume complete polarization. When the γ-rays are emitted perpendicular to the polarization direction of the source the intensity pattern is 3:4:1:1:4:3. Both σ and π components are linearly polarized, but their field vectors are oriented perpendicular to each other. An absorber which is perpendicularly polarized

with respect to the source will not absorb the incoming radiation at zero velocity (see, e.g., Fig. 6 of Ref.20). At resonance, $\Delta M = \pm 1$ transitions are induced which flip the polarization direction by 90° by changing σ into π components and vice versa. Thus the radiation emitted from a substate which was produced by a preceding NMR transition is again matched by the absorber and can produce Mössbauer absorption. When source and absorber are parallel polarized the same argumentation leads to the opposite expectation: decreasing Mössbauer absorption at resonance. The experimental data in Fig. 14 were intended to prove this prediction. Unfortunately, the effect for parallel polarization of source and absorber is still a slight increase of absorption, which we have to attribute to incomplete polarization. The polarizing field of 75 G at the source was certainly not enough to saturate the foil. The difference of the resonance effect between parallel and perpendicular polarization, however, is obvious and supports the above considerations. On the other hand, one should keep in mind that frequency modulation can also explain the difference between these two sets of data.

The experimental results presented in Figs. 10 to 13 were all carried out with source and absorber inside the rf-field and with H_0-fields, too low to polarize source and absorber in parallel. Thus, with a rather uncontrolled and probably not random polarization and rf-induced transitions in both source and absorber we face a complex situation which cannot serve to give an unambiguous understanding of the mechanism behind the experimentally observed effects. The difficulty is that due to the diminishing enhancement factor (see Eq. (16) the resonance disappears for large polarizing fields which would ensure a perfect polarization of the foils (compare Fig. 13). To

really ensure that the resonance effect represents NMR transitions more precise and conclusive experiments need to be done along two lines: 1) to use sources and absorbers which do not show magnetostriction; and 2) to do the experiments discussed above with single crystals which have well-defined magnetic axes.

In conclusion it can be said that the experimentally observed resonance effects have been interpreted as Mössbauer-NMR. Although this explanation is not unambiguously proved yet, strong arguments against frequency modulation effects arising from magnetostriction lead us to favor the interpretation in terms of NMR. If correct, this technique allows an absolute measurement of the hyperfine interaction in both the ground and excited state and does not suffer from calibration problems. Due to the line width problem Mössbauer-NMR applies only to cases with $\omega_0\tau \gg 1$ and $\omega_1\tau \gtrsim 0.1$ which prohibits its use in the nanosecond range. It is felt, however, that this method will acquire major importance for long-lived Mössbauer states which have hitherto been difficult to tackle.

ACKNOWLEDGMENTS

The results reviewed in this paper have been obtained in collaboration with several persons. B. Olsen (who also wrote the computer programs), D. A. Shirley, R. M. Steffen, and J. E. Templeton contributed significantly to the comprehension of angular correlation-NMR. For the Mössbauer-NMR D. Salomon carried the main burden of the experiments, and many elucidating discussions with M. P. Klein and D. A. Shirley led to the present understanding of the technique.

This work was done under the auspices of the U. S. Atomic Energy Commission.

REFERENCES AND FOOTNOTES

1. M. Deutsch and S. C. Brown, Phys. Rev. 85, 1047 (1952).
2. D. Connor, Phys. Rev. Letters 3, 429 (1959).
3. G. J. Perlow, Allerton Park Conference Report, University of Illinois (June 1960), unpublished.
4. K. Ziock, V. W. Hughes, R. Prepost, J. Baily, and W. Cleland, Phys. Rev. Letters 8, 103 (1962).
5. E. D. Commins and D. A. Dobson, Phys. Rev. Letters 10, 347 (1963).
6. K. Sugimoto, A. Mizobuchi, K. Nakai, and K. Matuda, Phys. Letters 18, 38 (1965) and J. Phys. Soc. Japan 21, 213 (1966).
7. E. Matthias, D. A. Shirley, M. P. Klein, and N. Edelstein, Phys. Rev. Letters 16, 974 (1966).
8. E. Matthias and R. J. Holiday, Phys. Rev. Letters 17, 897 (1966).
9. D. A. Shirley, Nuclear Orientation NMR, Proceedings of the Asimomar Conference.
10. E. Matthias, D. A. Shirley, N. Edelstein, H. J. Körner, and B. Olsen, Angular Correlation NMR in ^{100}Rh, Proceedings of the Asilomar Conference.
11. R. M. Steffen and H. Frauenfelder, Chapt. I in "Perturbed Angular Correlations," ed. by E. Kerlsson, E. Matthias and K. Siegbahn, North-Holland Publishing Company, Amsterdam 1964.
12. J. Brossel and F. Bitter, Phys. Rev. 86, 308 (1952).
13. M. N. Hack and M. Hamermesh, Il Nueovo Cimento XIX 546 (1961).
14. A. Abragam and R. V. Pound, Phys. Rev. 92, 943 (1953).
15. A. M. Portis and R. H. Lindquist, in Magnetism, ed. by G. T. Rado and R. Suhl (Academic Press, Inc. New York, 1965) Vol. IIA.

16. R. S. Preston, S. S. Hanna, and J. Heberle, Phys. Rev. 128, 2207 (1962).

17. The author is indebted to G. J. Perlow for pointing out this possibility.

18. S. L. Ruby and D. I. Bolef, Phys. Rev. Letters 5, 5 (1960).

19. This formula is valid for domains only.

20. U. Gonser, Mössbauer ^{57}Fe Polarimetry, Proceedings of the Asilomar Conference.

Table I. Historical review of experiments using nuclear radiation detection of NMR.

Authors	Year	Description of experiment	Type of radiation used
M. Deutsch and S. C. Brown[1]	1952	Hyperfine structure of positronium	annihilation radiation
D. Connor[2]	1959	$\mu(^{8}Li)$, following polarized thermal neutron capture	$^{8}Li \xrightarrow[0.8\ sec]{\beta^-} {}^{8}Be$
G. J. Perlow[3]	1960	NMR in ^{57m}Fe detected by its effect on Mössbauer absorption	γ(14.4 keV, 98 nsec)
K. Ziock, et al.[4]	1962	Hyperfine structure of muonium	β^+
E. D. Commins and D. A. Dobson[5]	1963	$\mu(^{19}Ne)$, following polarization in atomic beam apparatus	$^{19}Ne \xrightarrow[18\ sec]{\beta^+} {}^{19}F$
K. Sugimoto, et al.[6]	1965	$\mu(^{17}F)$, produced and polarized in $^{16}O(d,n)^{17}F$ reaction	$^{17}F \xrightarrow[66\ sec]{\beta^+} {}^{17}O$
E. Matthias, et al.[7]	1966	NMR in ^{100m}Rh, detected by its effect on angular correlation	γ(84-75 keV, 235 nsec)
E. Matthias and J. R. Holliday[8]	1966	NMR in ^{60}Co, polarized at low temperatures	γ(1.17 + 1.33 MeV, 5.3 years)

Table II. Form of angular correlation function for various geometries and $k_{max} = 2$ for random rf-phase. The angles refer to Fig. 1.

No.	θ_1	θ_2	$\phi_2-\phi_1$	$W(\vec{k}_1,\vec{k}_2,\vec{H}_0,\vec{H}_1)$
1	0°	180°		$1 + A_{22}\, G_{22}^{00}$
2	0°	90°	arbitr.	$1 - A_{22}\, \frac{1}{2} G_{22}^{00}$
3	0°	135°	arbitr.	$1 + A_{22}\, \frac{1}{4} G_{22}^{00}$
	45°	0°	arbitr.	
4	90°	90°	180°	$1 + A_{22}[\frac{1}{4} G_{22}^{00} + \frac{3}{8}(\mathrm{Re}G_{22}^{22} + \mathrm{Re}G_{22}^{-2-2})]$
5	90°	90°	90°	$1 + A_{22}[\frac{1}{4} G_{22}^{00} - \frac{3}{8}(\mathrm{Re}G_{22}^{22} + \mathrm{Re}G_{22}^{-2-2})]$
6	90°	90°	-135°	$1 + A_{22}[\frac{1}{4} G_{22}^{00} - \frac{3}{8}(\mathrm{Im}G_{22}^{22} - \mathrm{Im}G_{22}^{-2-2})]$
			45°	
7	90°	90°	135°	$1 + A_{22}[\frac{1}{4} G_{22}^{00} + \frac{3}{8}(\mathrm{Im}G_{22}^{22} - \mathrm{Im}G_{22}^{-2-2})]$
			-45°	

Table III. Form of angular correlation function for various geometries, $k_{max} = 2$, and fixed rf-phase $\Delta = 0$. The angles refer to Fig. 1.

No.	Θ_1	ϕ_1	Θ_2	ϕ_2	$W(\vec{k}_1,\vec{k}_2,\vec{H}_0,\vec{H}_1)$
1	0°	0°	180°	0°	$1 + A_{22}G_{22}^{00}$
2	0°	0°	90°	90°	$1 - A_{22}[\frac{1}{2}G_{22}^{00} + \sqrt{\frac{3}{8}}(\mathrm{Re}G_{22}^{02} + \mathrm{Re}G_{22}^{0-2})]$
3	0°	0°	90°	0°	$1 - A_{22}[\frac{1}{2}G_{22}^{00} - \sqrt{\frac{3}{8}}(\mathrm{Re}G_{22}^{02} + \mathrm{Re}G_{22}^{0-2})]$
4	0°	0°	90°	45°	$1 - A_{22}[\frac{1}{2}G_{22}^{00} + \sqrt{\frac{3}{8}}(\mathrm{Im}G_{22}^{02} - \mathrm{Im}G_{22}^{0-2})]$
5	90°	45°	0°	0°	$1 - A_{22}[\frac{1}{2}G_{22}^{00} - \sqrt{\frac{3}{8}}(\mathrm{Im}G_{22}^{20} - \mathrm{Im}G_{22}^{-20})]$
6	90°	135°	0°	0°	$1 - A_{22}[\frac{1}{2}G_{22}^{00} + \sqrt{\frac{3}{8}}(\mathrm{Im}G_{22}^{20} - \mathrm{Im}G_{22}^{-20})]$
7	0°	0°	135°	90°	$1 + A_{22}[\frac{1}{4}G_{22}^{00} - \sqrt{\frac{3}{8}}(\mathrm{Im}G_{22}^{01} + \mathrm{Im}G_{22}^{0-1}) - \sqrt{\frac{3}{32}}(\mathrm{Re}G_{22}^{02} + \mathrm{Re}G_{22}^{0-2})]$
8	45°	90°	0°	0°	$1 + A_{22}[\frac{1}{4}G_{22}^{00} - \sqrt{\frac{3}{8}}(\mathrm{Im}G_{22}^{10} + \mathrm{Im}G_{22}^{-10}) - \sqrt{\frac{3}{32}}(\mathrm{Re}G_{22}^{20} + \mathrm{Re}G_{22}^{-20})]$
9	90°	0°	90°	180°	$1 + A_{22}[\frac{1}{4}G_{22}^{00} - \sqrt{\frac{3}{32}}(\mathrm{Re}G_{22}^{02} + \mathrm{Re}G_{22}^{0-2} + \mathrm{Re}G_{22}^{20} + \mathrm{Re}G_{22}^{-20}) + \frac{3}{8}(\mathrm{Re}G_{22}^{22} + \mathrm{Re}G_{22}^{2-2} + \mathrm{Re}G_{22}^{-22} + \mathrm{Re}G_{22}^{-2-2})]$
10	90°	0°	90°	135°	$1 + A_{22}[\frac{1}{4}G_{22}^{00} - \sqrt{\frac{3}{32}}(\mathrm{Im}G_{22}^{02} - \mathrm{Im}G_{22}^{0-2} + \mathrm{Re}G_{22}^{20} + \mathrm{Re}G_{22}^{-20}) + \frac{3}{8}(\mathrm{Im}G_{22}^{22} - \mathrm{Im}G_{22}^{2-2} + \mathrm{Im}G_{22}^{-22} - \mathrm{Im}G_{22}^{-2-2})]$
11	90°	45°	90°	135°	$1 + A_{22}[\frac{1}{4}G_{22}^{00} - \sqrt{\frac{3}{32}}(\mathrm{Im}G_{22}^{02} - \mathrm{Im}G_{22}^{0-2} + \mathrm{Im}G_{22}^{20} - \mathrm{Im}G_{22}^{-20}) - \frac{3}{8}(\mathrm{Re}G_{22}^{22} - \mathrm{Re}G_{22}^{2-2} - \mathrm{Re}G_{22}^{-22} + \mathrm{Re}G_{22}^{-2-2})]$
12	90°	45°	90°	0°	$1 + A_{22}[\frac{1}{4}G_{22}^{00} - \sqrt{\frac{3}{32}}(\mathrm{Re}G_{22}^{02} + \mathrm{Re}G_{22}^{0-2} + \mathrm{Im}G_{22}^{20} - \mathrm{Im}G_{22}^{-20}) + \frac{3}{8}(\mathrm{Im}G_{22}^{22} + \mathrm{Im}G_{22}^{2-2} - \mathrm{Im}G_{22}^{-22} - \mathrm{Im}G_{22}^{-2-2})]$
13	90°	90°	90°	45°	$1 + A_{22}[\frac{1}{4}G_{22}^{00} + \sqrt{\frac{3}{32}}(\mathrm{Im}G_{22}^{02} - \mathrm{Im}G_{22}^{0-2} - \mathrm{Re}G_{22}^{20} + \mathrm{Re}G_{22}^{-20}) - \frac{3}{8}(\mathrm{Im}G_{22}^{22} - \mathrm{Im}G_{22}^{2-2} - \mathrm{Im}G_{22}^{-22} + \mathrm{Im}G_{22}^{-2-2})]$

FIGURE CAPTIONS

Fig. 1. Axis system and definition of angles for angular correlation-NMR.

Fig. 2. Form of angular correlation resonance for $k_{max} = 2$ and random rf-phase.

Fig. 3. Form of the $k = 4$ term in angular correlation-MMR for random rf-phase.

Fig. 4. Perturbation factors $\hat{G}_{kk}^{00}$ at resonance (random rf-phase) as a function of $|\omega_0\tau|$ for three parameters values H_1/H_0. The missing $\hat{G}_{44}^{00}$ curves for $H_1/H_0 = 10^{-2}$ and 10^{-4} can be constructed by using the same shift as for the $\hat{G}_{22}^{00}$ curves.

Fig. 5. Perturbation factor expected for the indicated geometry when pulsed rf is used with a fixed phase $\Delta = 0$ at time zero. The shift of the resonance when observed at two different angles (45° and 135°) should permit a relative sign determination.

Fig. 6. Perturbation factor for some values of $\omega_0\tau$ for the indicated geometry and pulsed rf with fixed phase $\Delta = 0$ at time zero. The opposite sign of the resonance for opposite signs of $\omega_0\tau$ can be used to determine the relative sign of $\omega_0\tau$.

Fig. 7. Perturbation factor for some values of $\omega_0\tau$ and pulsed rf ($\Delta = 0$) for the simple geometry shown.

Fig. 8. An unsplit resonance as can be found in this particular geometry with pulsed rf ($\Delta = 0$). This geometry is very favorable for beam experiments.

Fig. 9. Perturbation factor for another favorable beam geometry, pulsed rf ($\Delta = 0$) and some values of $\omega_0\tau$. Again the shift of the resonance offers the possibility of a relative sign determination.

Fig. 10. Frequency spectrum observed in transmission at zero velocity with both source and absorber exposed to the rf-field. An increase of absorption is measured at the nuclear resonance frequencies for the ground and excited state.

Fig. 11. Resonance of the 14.4 keV state observed in transmission at zero velocity with source and absorber in the rf-field.

Fig. 12. Resonance of the ground state observed in transmission at zero velocity with source and absorber in the rf-field.

Fig. 13. Frequency spectrum about the excited state resonance for various polarizing fields H_0. Here, V_1 is the voltage across the rf-coil. Source and absorber were sandwiched together inside the rf-field.

Fig. 14. Comparison of the frequency spectrum for parallel and perpendicular polarization of source and absorber. Only the source was inside the rf-field.

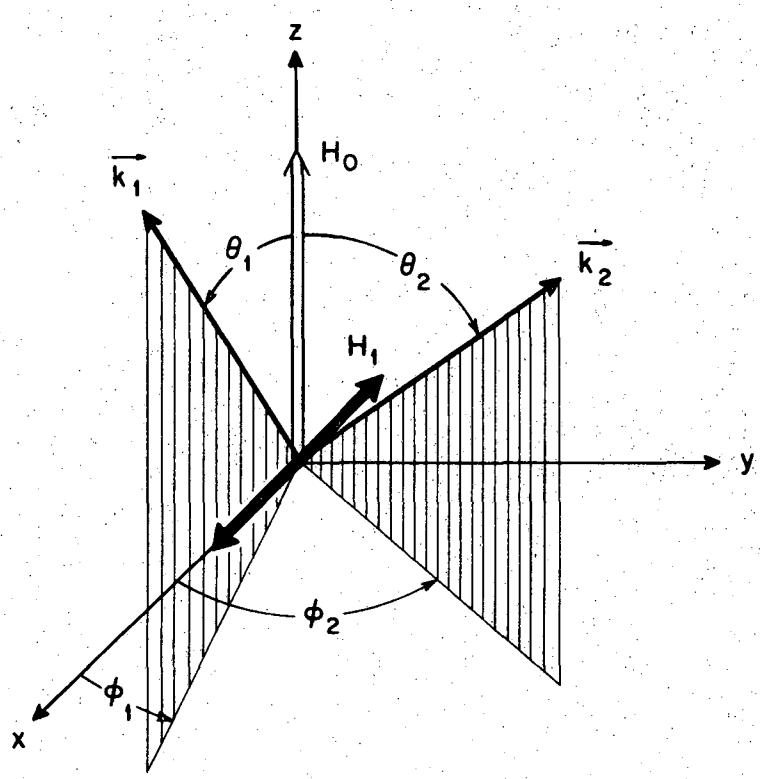

XBL678-3906

Fig. 1

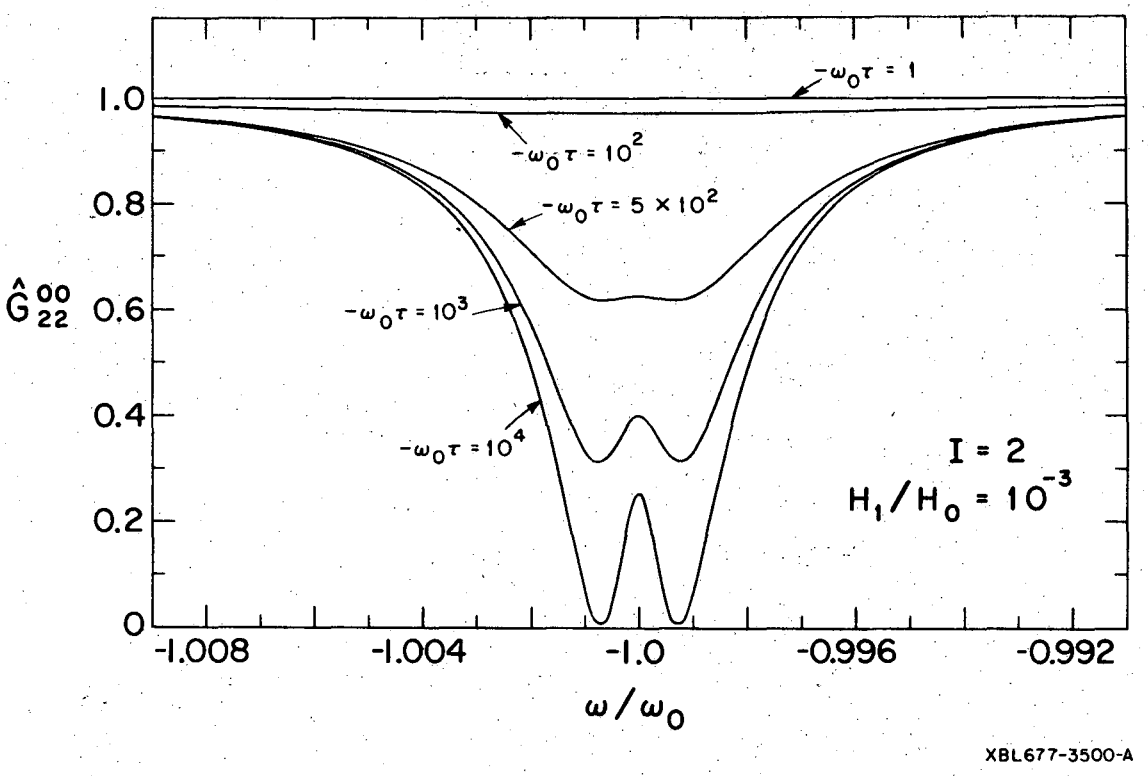
$-\omega_0\tau = 1$
$-\omega_0\tau = 10^2$
$-\omega_0\tau = 5 \times 10^2$
$-\omega_0\tau = 10^3$
$-\omega_0\tau = 10^4$
I = 2
$H_1/H_0 = 10^{-3}$
$\hat{G}^{00}_{22}$
1.0
0.8
0.6
0.4
0.2
0
-1.008
-1.004
-1.0
-0.996
-0.992
ω/ω_0
XBL677-3500-A

Fig. 2

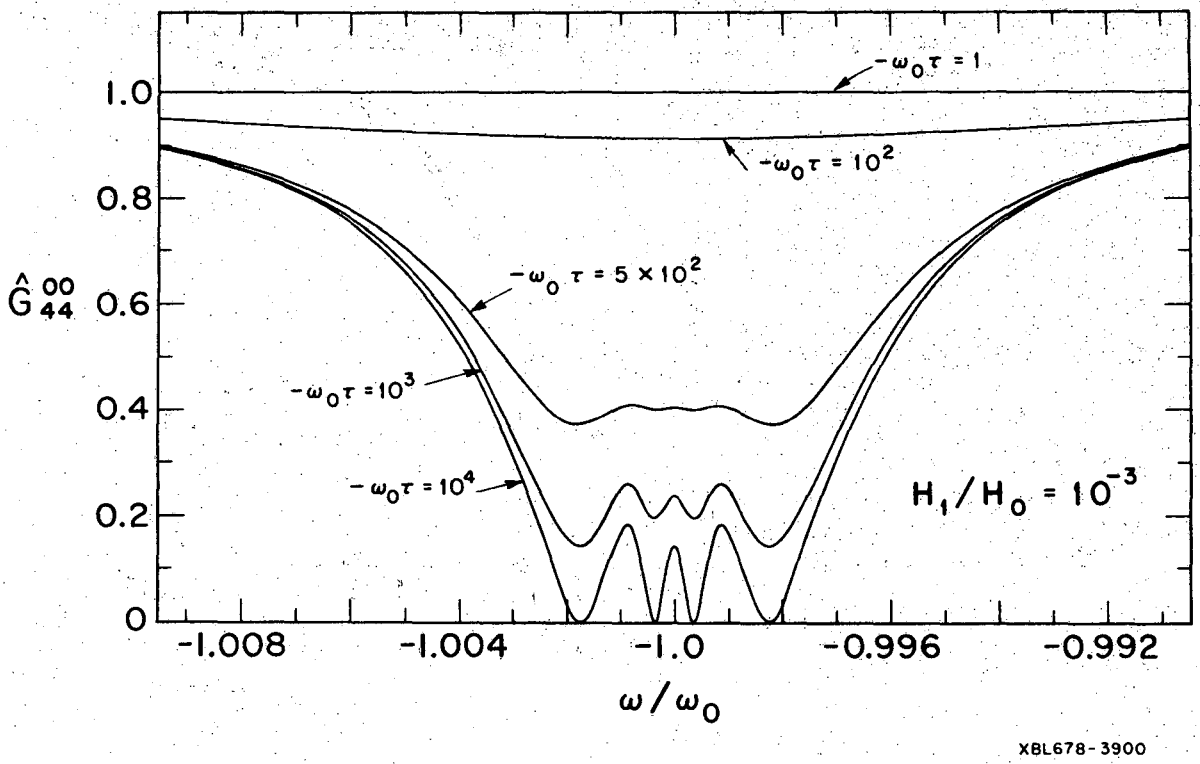
$-\omega_0\tau = 1$
$-\omega_0\tau = 10^2$
$-\omega_0\tau = 5\times10^2$
$-\omega_0\tau = 10^3$
$-\omega_0\tau = 10^4$
$H_1/H_0 = 10^{-3}$
$\hat{G}^{00}_{44}$
1.0
0.8
0.6
0.4
0.2
0
-1.008
-1.004
-1.0
-0.996
-0.992
ω/ω_0
XBL678-3900

Fig. 3

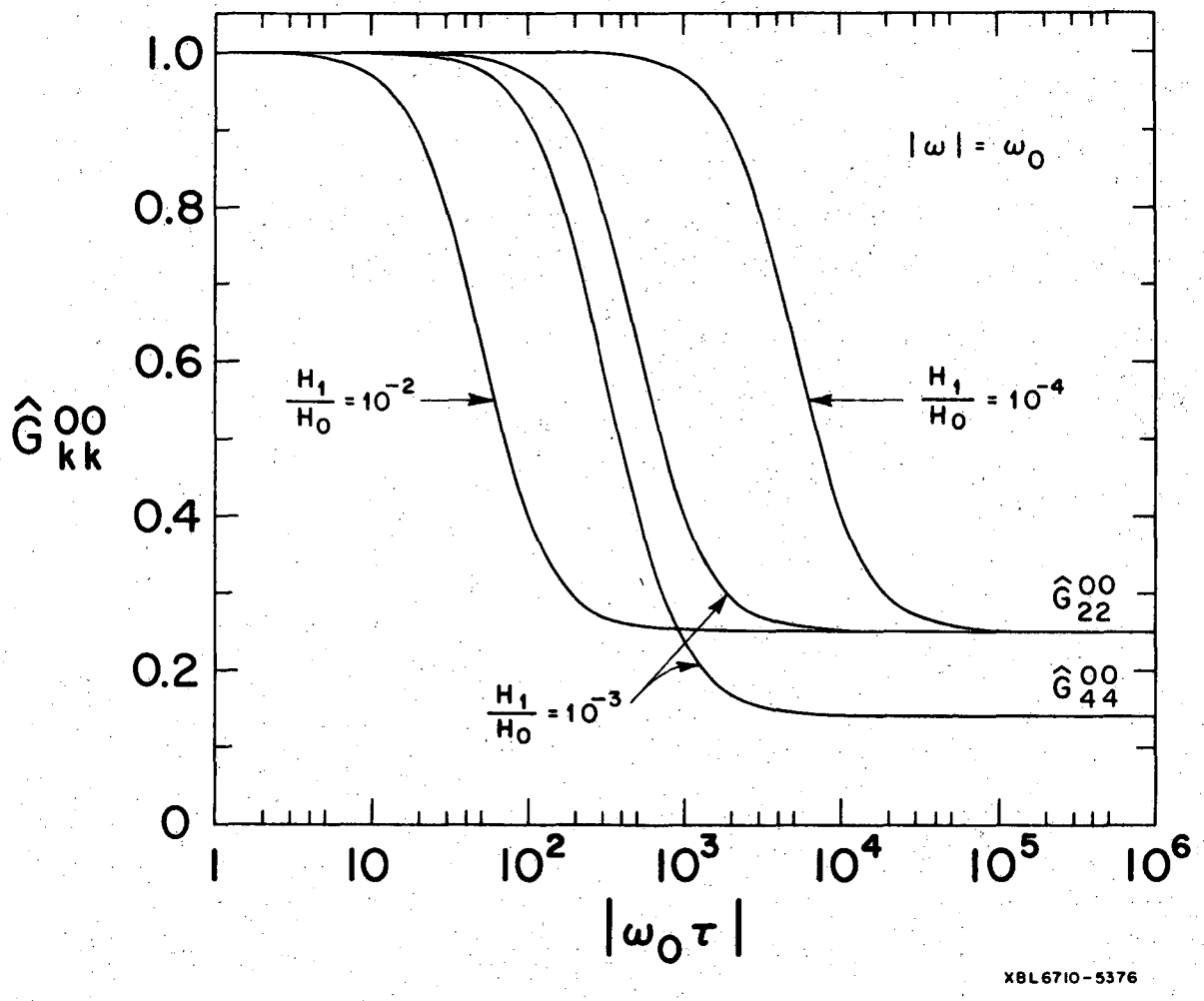
1.0
0.8
0.6
0.4
0.2
0
$\hat{G}^{00}_{kk}$
$|\omega| = \omega_0$
$\frac{H_1}{H_0} = 10^{-2}$
$\frac{H_1}{H_0} = 10^{-4}$
$\frac{H_1}{H_0} = 10^{-3}$
$\hat{G}^{00}_{22}$
$\hat{G}^{00}_{44}$
1
10
10^2
10^3
10^4
10^5
10^6
$|\omega_0 \tau|$
XBL6710-5376

Fig. 4

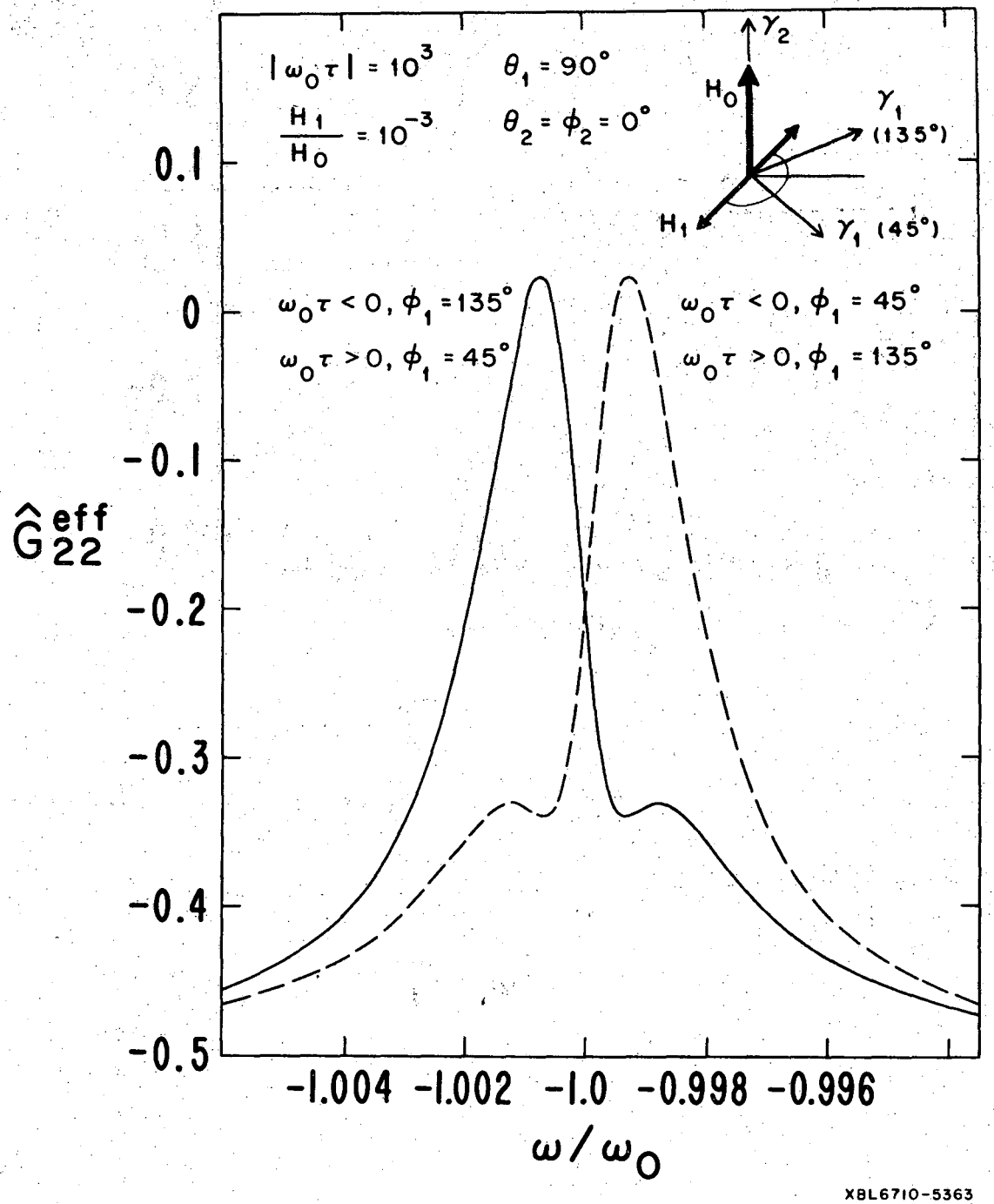
$|\omega_0\tau| = 10^3$
$\frac{H_1}{H_0} = 10^{-3}$
$\theta_1 = 90°$
$\theta_2 = \phi_2 = 0°$
γ_2
H_0
γ_1 (135°)
H_1
γ_1 (45°)
$\omega_0\tau < 0, \phi_1 = 135°$
$\omega_0\tau > 0, \phi_1 = 45°$
$\omega_0\tau < 0, \phi_1 = 45°$
$\omega_0\tau > 0, \phi_1 = 135°$
$\hat{G}^{eff}_{22}$
0.1
0
-0.1
-0.2
-0.3
-0.4
-0.5
-1.004 -1.002 -1.0 -0.998 -0.996
ω/ω_0
XBL6710-5363

Fig. 5

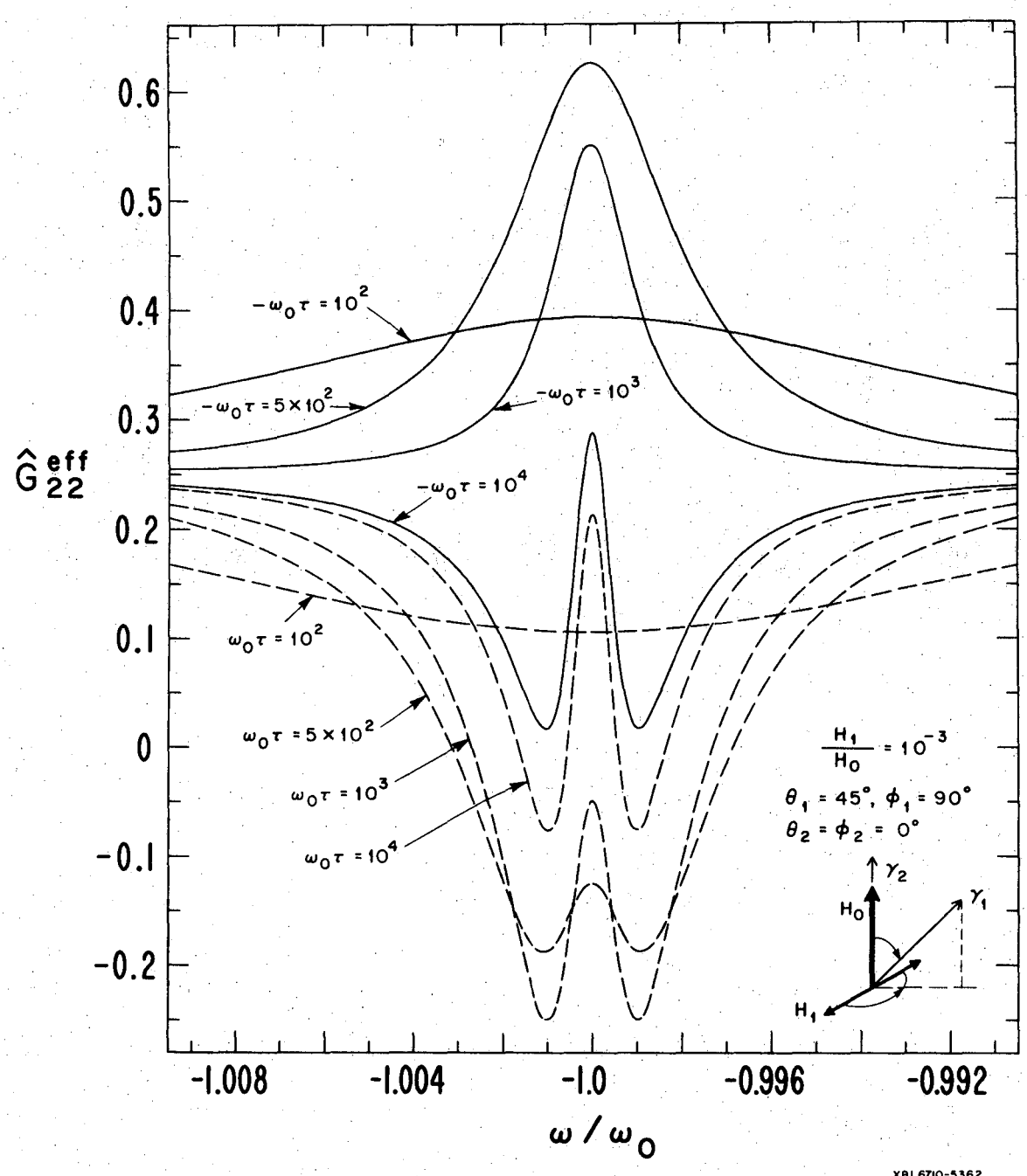
0.6
0.5
0.4
0.3
0.2
0.1
0
-0.1
-0.2
$\hat{G}^{eff}_{22}$
$-\omega_0\tau = 10^2$
$-\omega_0\tau = 5\times10^2$
$-\omega_0\tau = 10^3$
$-\omega_0\tau = 10^4$
$\omega_0\tau = 10^2$
$\omega_0\tau = 5\times10^2$
$\omega_0\tau = 10^3$
$\omega_0\tau = 10^4$
$\frac{H_1}{H_0} = 10^{-3}$
$\theta_1 = 45°, \phi_1 = 90°$
$\theta_2 = \phi_2 = 0°$
γ_2
H_0
γ_1
H_1
-1.008
-1.004
-1.0
-0.996
-0.992
ω / ω_0
XBL6710-5362

Fig. 6

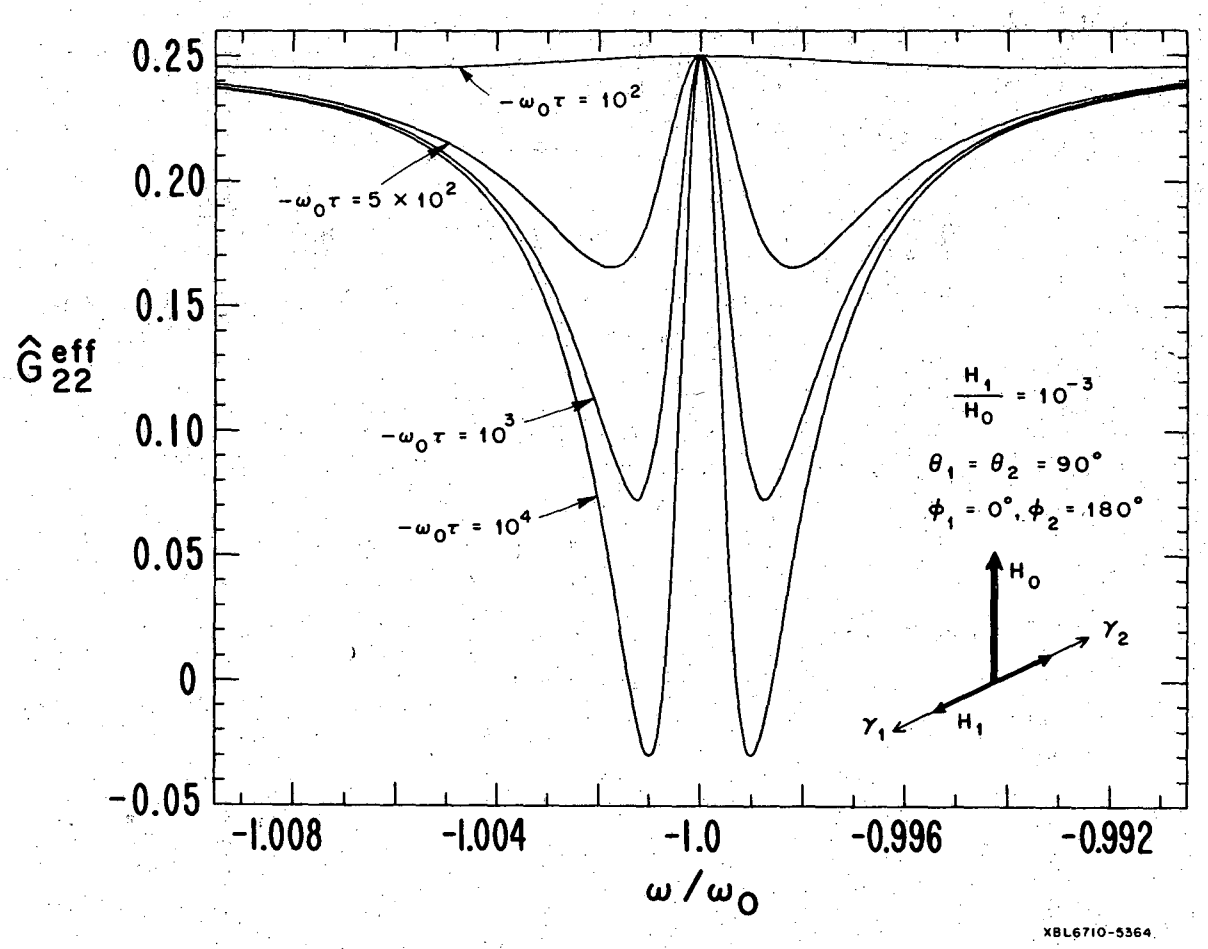
0.25
0.20
0.15
0.10
0.05
0
-0.05
$\hat{G}_{22}^{eff}$
$-\omega_0\tau = 10^2$
$-\omega_0\tau = 5 \times 10^2$
$-\omega_0\tau = 10^3$
$-\omega_0\tau = 10^4$
$\frac{H_1}{H_0} = 10^{-3}$
$\theta_1 = \theta_2 = 90°$
$\phi_1 = 0°, \phi_2 = 180°$
H_0
γ_2
γ_1
H_1
-1.008
-1.004
-1.0
-0.996
-0.992
ω / ω_0
XBL6710-5364

Fig. 7

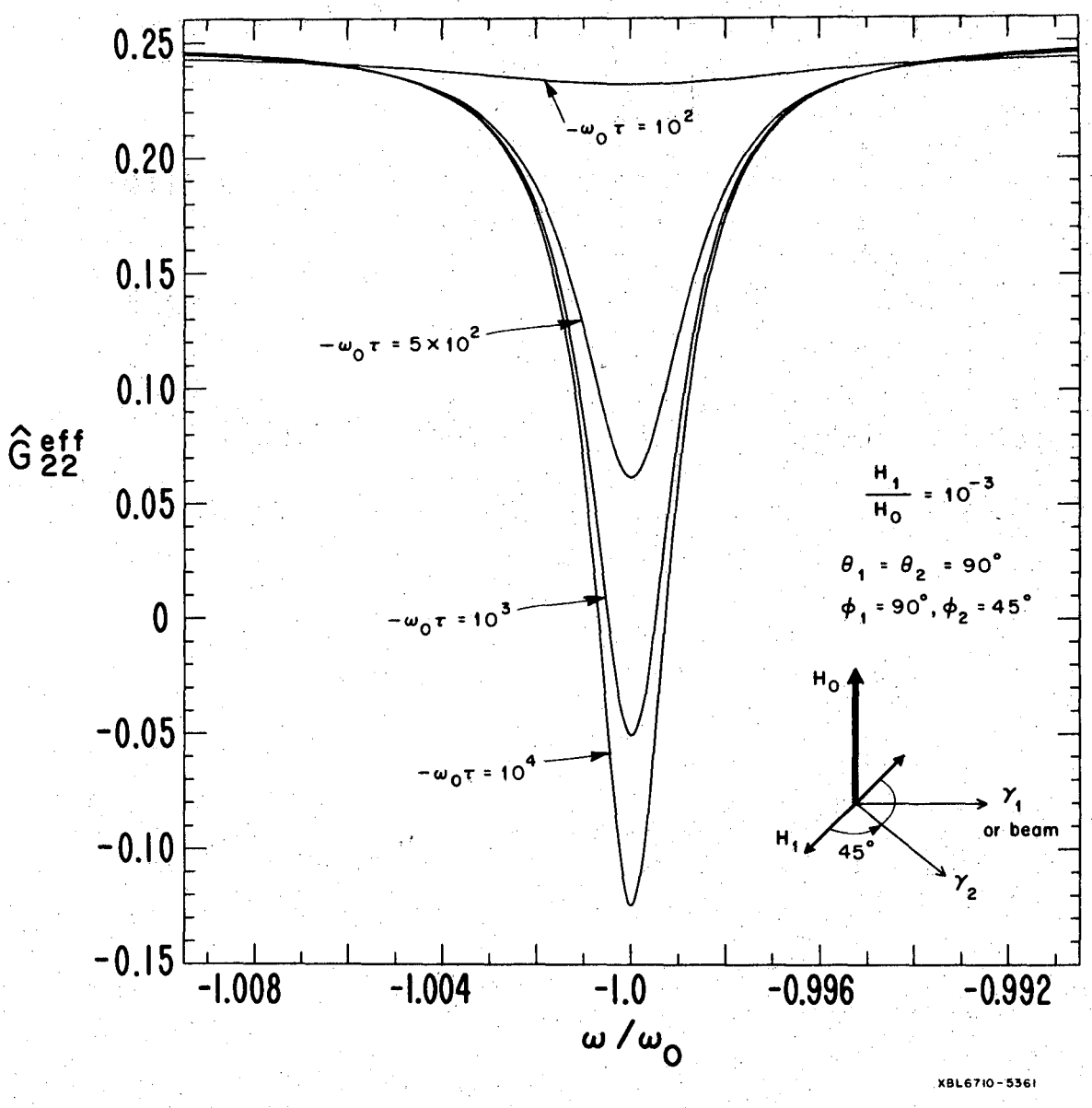
0.25
0.20
0.15
0.10
0.05
0
-0.05
-0.10
-0.15
$\hat{G}^{eff}_{22}$
$-\omega_0\tau = 10^2$
$-\omega_0\tau = 5\times10^2$
$-\omega_0\tau = 10^3$
$-\omega_0\tau = 10^4$
$\frac{H_1}{H_0} = 10^{-3}$
$\theta_1 = \theta_2 = 90°$
$\phi_1 = 90°, \phi_2 = 45°$
H_0
H_1
45°
γ_1
or beam
γ_2
-1.008
-1.004
-1.0
-0.996
-0.992
ω/ω_0
XBL6710-5361

Fig. 8

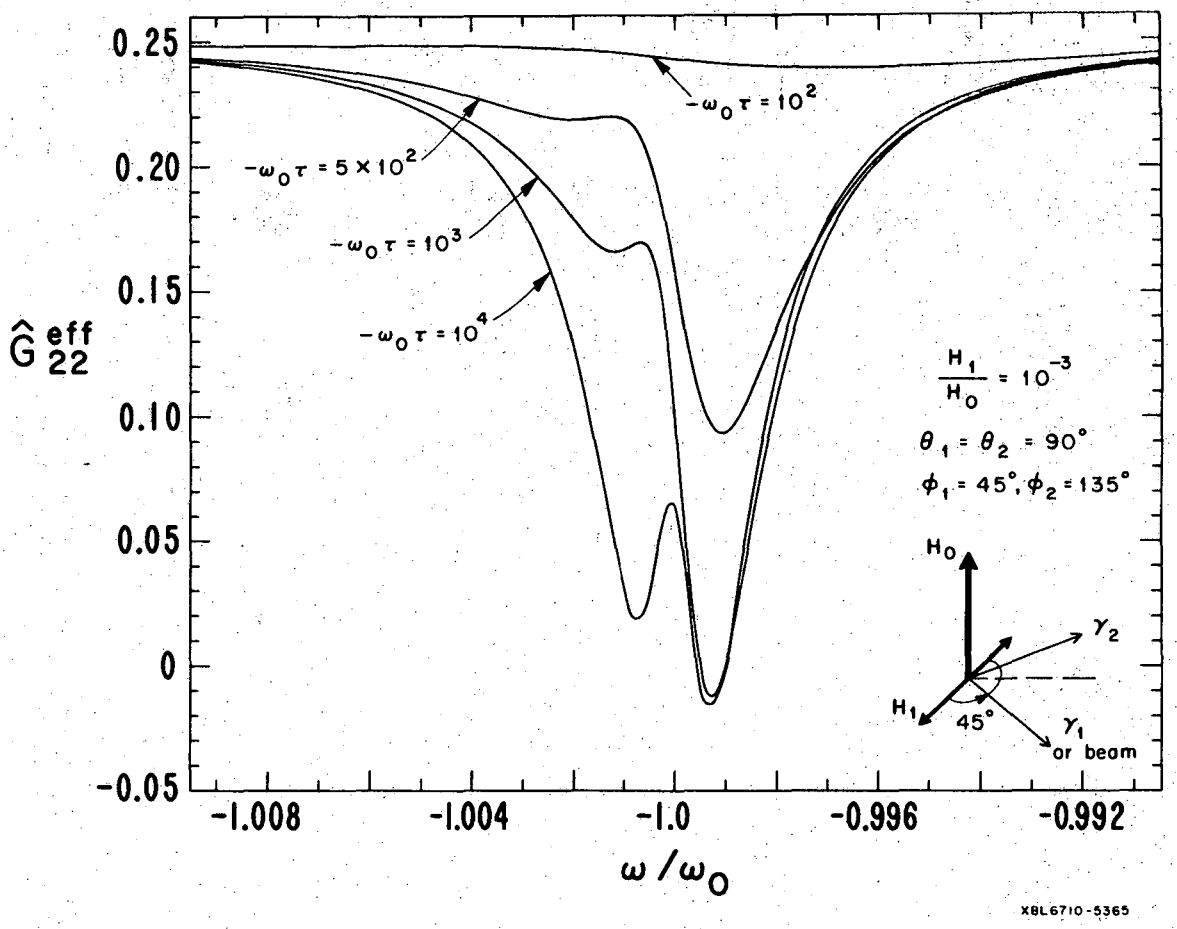
0.25
0.20
0.15
0.10
0.05
0
-0.05
$\hat{G}^{eff}_{22}$
$-\omega_0\tau = 10^2$
$-\omega_0\tau = 5\times10^2$
$-\omega_0\tau = 10^3$
$-\omega_0\tau = 10^4$
$\frac{H_1}{H_0} = 10^{-3}$
$\theta_1 = \theta_2 = 90°$
$\phi_1 = 45°, \phi_2 = 135°$
H_0
γ_2
H_1
45°
γ_1
or beam
-1.008
-1.004
-1.0
-0.996
-0.992
ω/ω_0
XBL6710-5365

Fig. 9

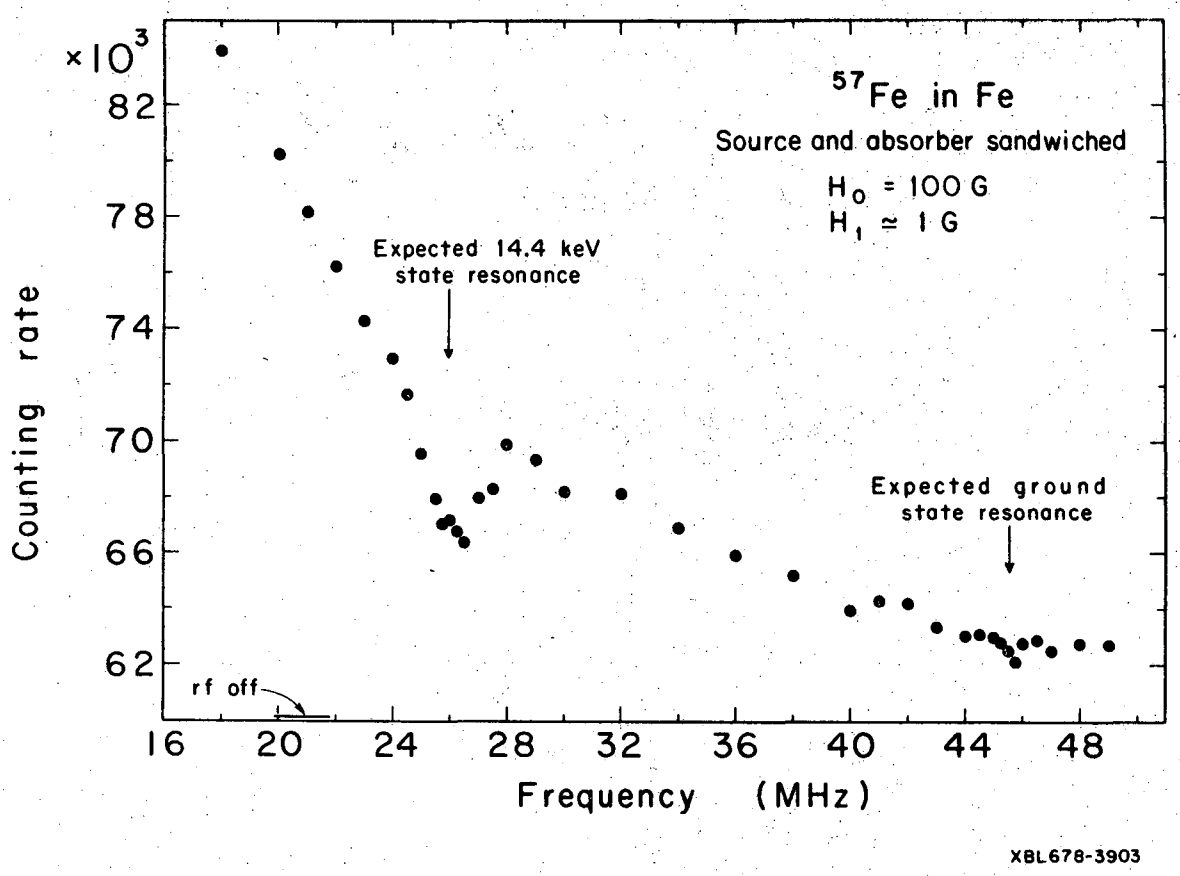
×10³
82
78
74
70
66
62
Counting rate
57Fe in Fe
Source and absorber sandwiched
H0 = 100 G
H1 ≃ 1 G
Expected 14.4 keV
state resonance
Expected ground
state resonance
rf off
16
20
24
28
32
36
40
44
48
Frequency (MHz)
XBL678-3903

Fig. 10

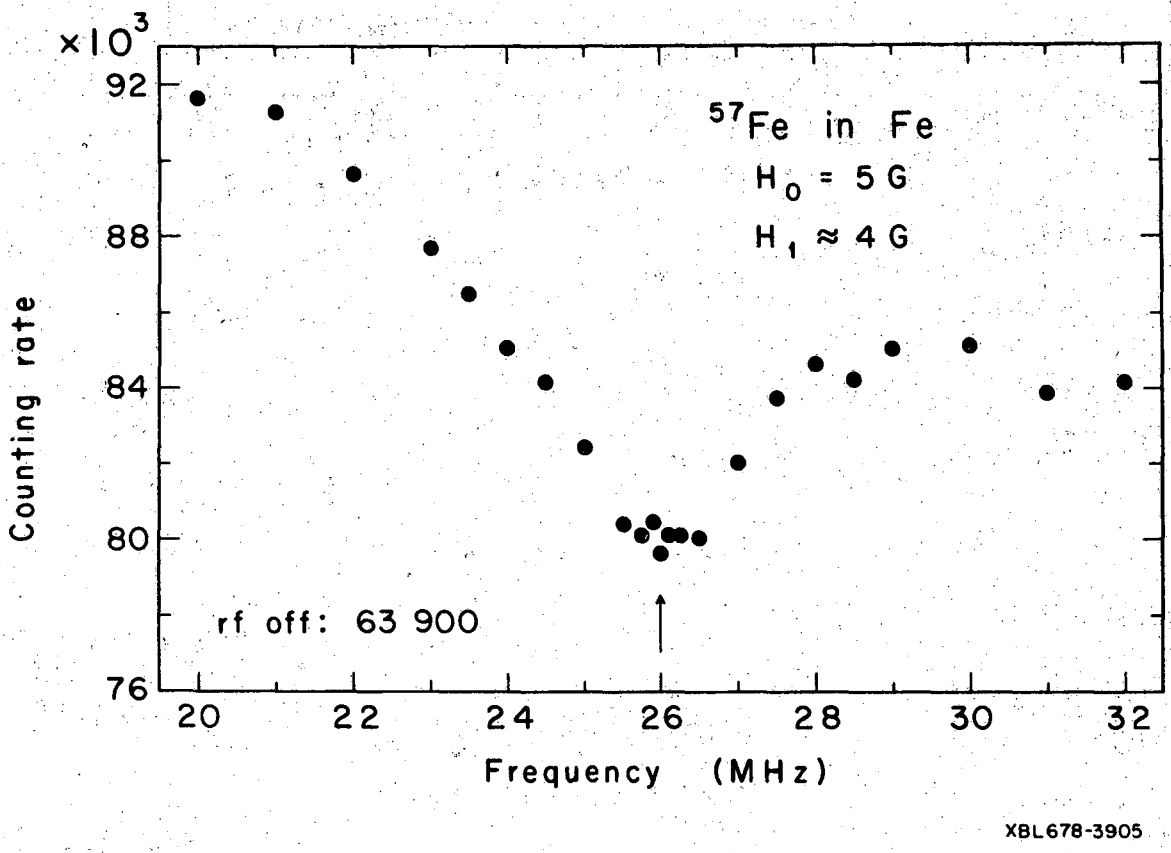
×10³
92
88
84
80
76
Counting rate
⁵⁷Fe in Fe
H₀ = 5 G
H₁ ≈ 4 G
rf off: 63 900
20
22
24
26
28
30
32
Frequency (MHz)
XBL678-3905

Fig. 11

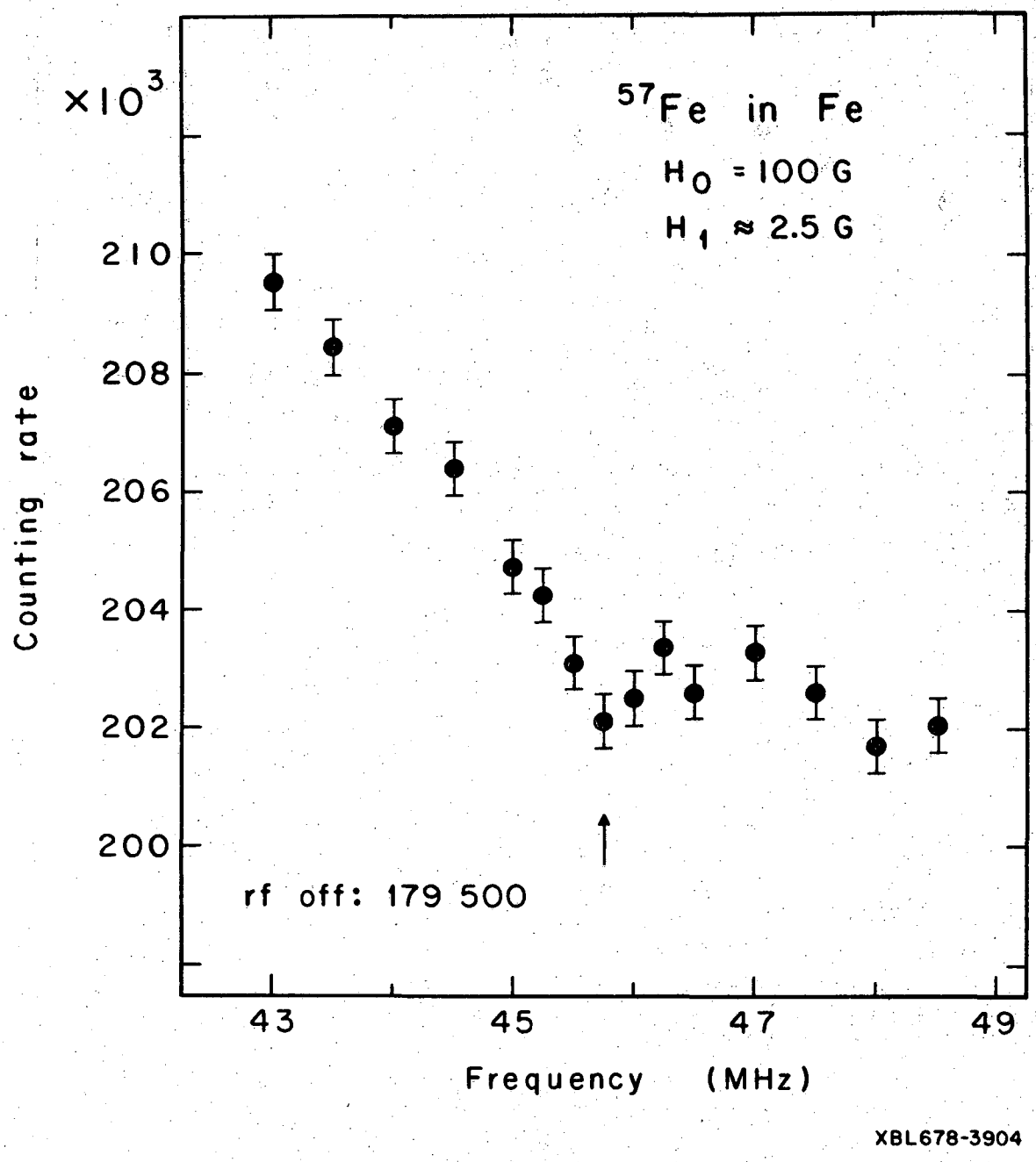
×10³
210
208
206
204
202
200
Counting rate
⁵⁷Fe in Fe
H₀ = 100 G
H₁ ≈ 2.5 G
rf off: 179 500
43
45
47
49
Frequency (MHz)
XBL678-3904

Fig. 12

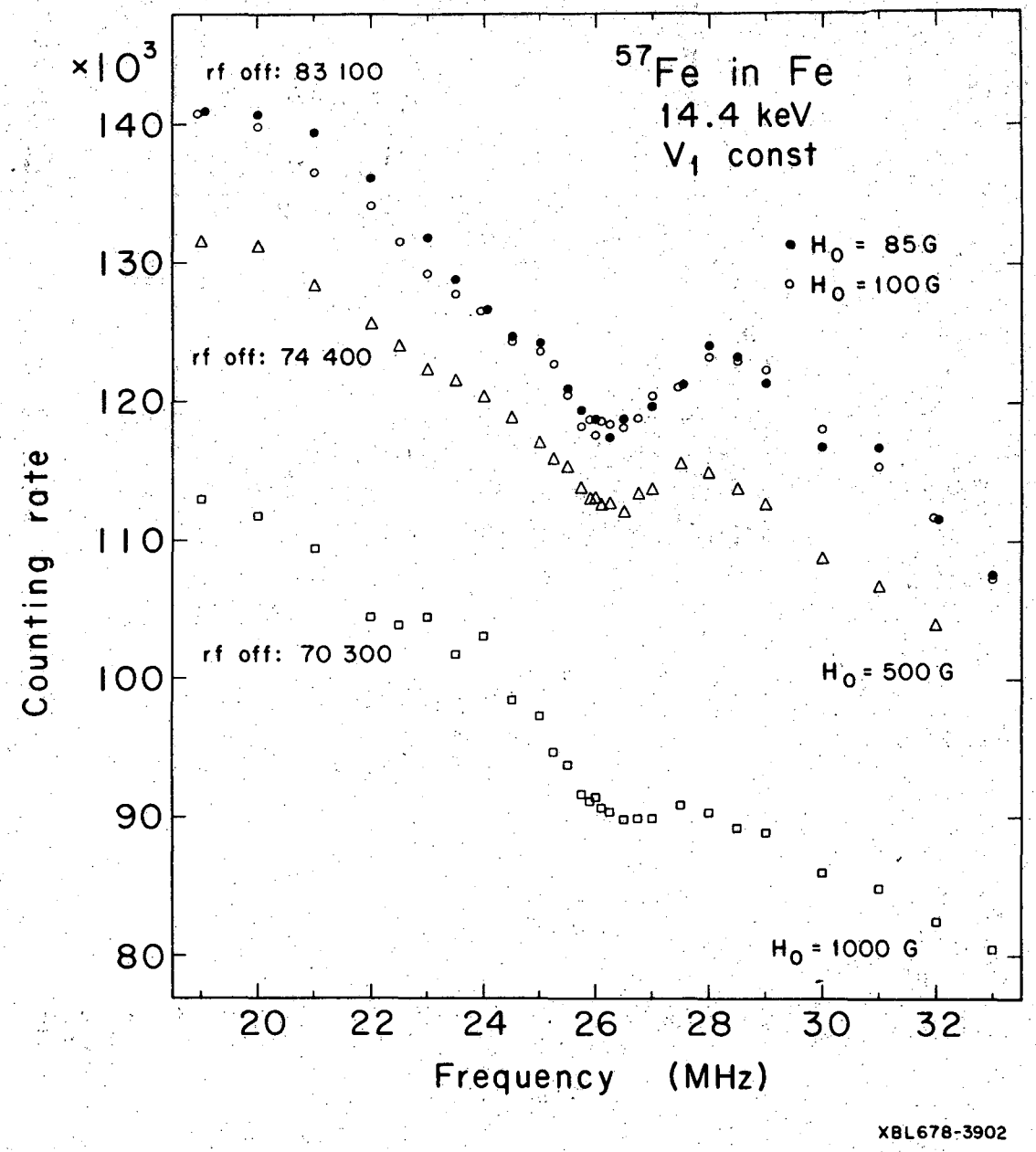
×10³
140
130
120
110
100
90
80
Counting rate
rf off: 83 100
rf off: 74 400
rf off: 70 300
⁵⁷Fe in Fe
14.4 keV
V₁ const
• H₀ = 85 G
○ H₀ = 100 G
H₀ = 500 G
H₀ = 1000 G
20
22
24
26
28
30
32
Frequency (MHz)
XBL678-3902

Fig. 13

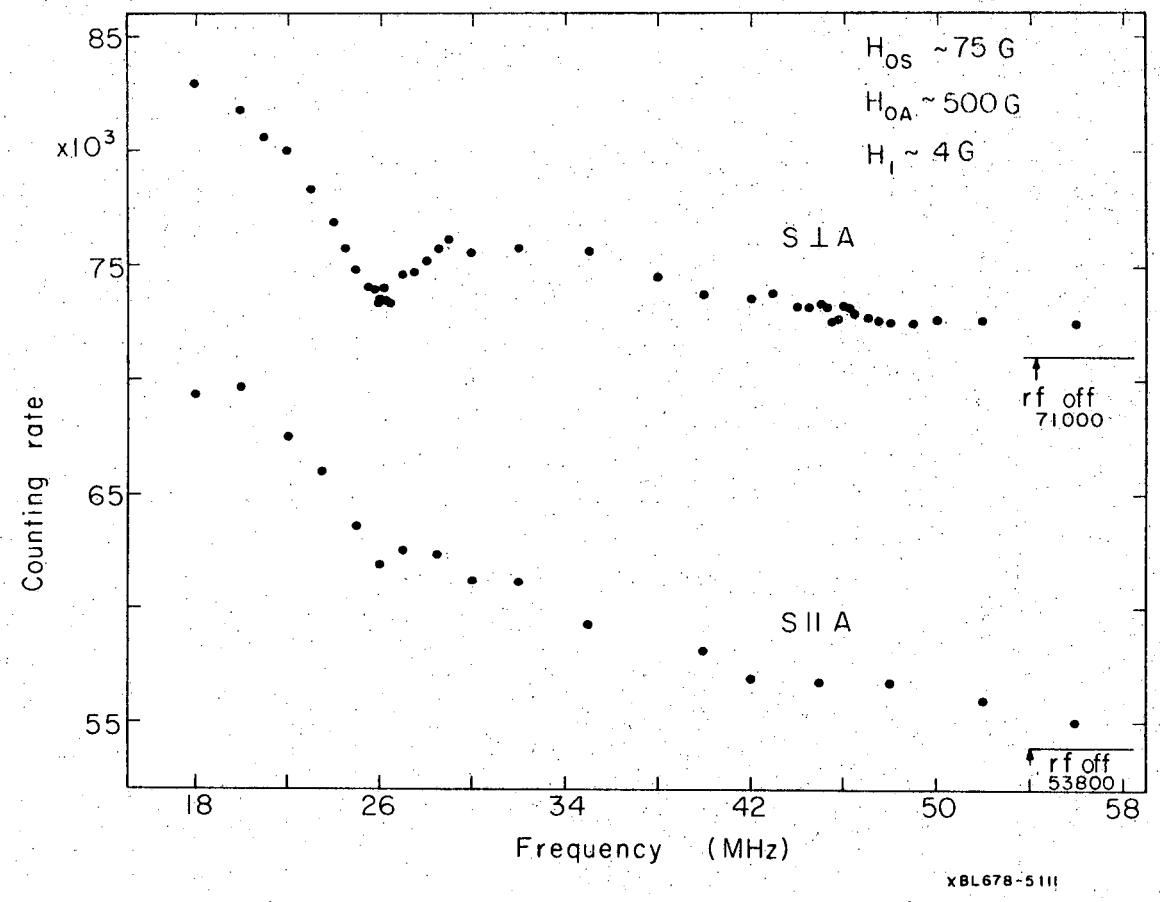
85
x10³
75
65
55
Counting rate
18
26
34
42
50
58
Frequency (MHz)
H_OS ~75 G
H_OA ~500 G
H_1 ~ 4 G
S ⊥ A
S II A
rf off
71000
rf off
53800
XBL678-5111

Fig. 14